Results in Physics 5 (2015) 85–91

Contents lists available at ScienceDirect

Results in Physics

journal homepage: www.journals.elsevier.com/results-in-physics

Plasma parameters in 40 MHz Argon discharge

A.A. Azooz [a,*], S. Cakir [b], D.A. Bleej [c]

[a] Department of Physics, College of Science, Mosul University, Mosul, Iraq
[b] Department of Physics, Middle East Technical University, Ankara, Turkey
[c] Department of Physics, Faculty of Science, Zakho University, Zakho, Iraq

ARTICLE INFO

Article history:
Received 30 November 2014
Accepted 19 January 2015
Available online 29 January 2015

Keywords:
Automated plasma diagnostics
Double probe
Argon plasma
Langmuir probe
Spectroscopic plasma diagnostics
40 GHz RF plasma

ABSTRACT

Experimental data related to 40 MHz Argon plasma parameters in the RF power and pressure ranges of 25–200 W and 0.2–0.5 Torr are presented. Electron temperatures are obtained using both double probe and optical spectroscopy methods. Acceptable consistency between results is obtained. Double probe method is also used to obtain the plasma electron density. At any particular pressure value, the effect of increasing RF power seems to be restricted to increasing plasma electron density rather than affecting the plasma electron temperatures. Signature of the Paschen law effect is reflected on the relation between pressure and electron plasma density.

Introduction

Radio frequency (RF) plasma discharge has become a major part of low temperature plasma physics research and applications. This is mainly due to several advantages related to plasma parameters control compared to DC discharge. It is rather unfortunate that the only three RF bands allocated for industrial, scientific and medical (ISM) that can be used worldwide by the International Telecommunications Authority are the 13.56, its second harmonic 27.12 and 40.68 MHz radio frequencies [1]. Some experimental works have been performed at other frequencies [2–5] but only inside highly RF shielded advanced laboratories which is not the case in most other plasma physics labs. Some simulation works on the frequency effects on the discharge have also been carried out [6,7]. It is believed that some more interesting RF discharge physics may have come to light if other RF frequencies were available in this field. Most of the RF plasma discharge studies are conducted using the 13.56 MHz [8–16]. Some modeling of the frequency effect on RF discharge properties has demonstrated that the anomalous skin effect plays an important role in changing the ratio of the total to the collisional RF absorbed power. The results show that this ratio is at maximum at frequency of about 9 MHz [17]. This is close to the standard 13.6 MHz used in most RF discharge research. Extensive search for the literature indicated that there are far fewer works carried out at 40.68 MHz compared to those at 13.56 MHz.

It is the purpose here to present some experimental data related to RF power and pressure plasma parameters dependence in Argon using 40.68 MHz. From plasma deposition applications point of view, this frequency is considered interesting. This is because it is known to produce significantly higher deposition rates compared to the 13.56 MHz [18–20].

Experimental setup

The experimental setup used in this work is shown in Fig. 1. It consists of a 400 mm diameter 500 mm height stainless steel cylindrical reactor. The reactor contains two circular 200 mm in diameter, well polished aluminum electrodes. The electrodes are Teflon insulated on the rims and the sides not facing the discharge in order to prevent any auxiliary discharges with the chamber walls. The reactor has several flanged ports. These ports are used for vacuum pump, vacuum gauge, gas feed, probe connection, and spectrometer fiber optics cable connections.

Two types of plasma diagnostic techniques are employed. The first is the double probe technique. This probe is automated Langmuir probe system (ALP) made by Impedance company [21]. The double probe consists of two 2 mm in length and 0.5 mm in diameter tungsten probe tips mounted in a push-fit cradle, a ceramic-coated probe shaft, integrated re-entrant ceramic feed through, flange. The probe associated electronics involve a sweep generator, data acquisition device, and necessary software. Although the built in software do produce automated results related to plasma parameters from the measured I–V

* Corresponding author.

http://dx.doi.org/10.1016/j.rinp.2015.01.005
2211-3797/

Fig. 1. Experimental setup.

characteristics, it was decided at some stage that an independent analysis of the raw data measured by the system will produce more self consistent results. This will be discussed further later. Typical raw data produced by the system are shown in Fig. 2. The red points are the raw experimental data measured. The white dashed line is the fit carried out by the internally built in software. The numerical results on the right are the plasma parameters obtained from such fit. However, these automated numerical results are not included in this work because of the large deviations between acquired data and the fitted curve. Alternatively, the raw numerical data (red dots) are saved and fitted to a more suitable empirical formula to obtain the correct values for the plasma electron temperature and density.

In conjunction with the double probe system, spectroscopic measurements on the generated plasma are carried out using Ocean Optic HR2000 High-resolution Miniature Fiber Optic Spectrometer [22] with a spectral range 200–1100 nm. Spectra of the RF plasmas were measured directly using a fiber optic cable fed through one of the ports of the vacuum chamber. Acquired data of all spectra under the studied experimental conditions are converted to MATLAB data files for further line ratio analysis. Typical spectrum obtained at 0.2 Torr, 150 W is shown in Fig. 3.

Data and analysis

Both spectroscopic and double probe data are used to estimate the plasma electron temperatures as a function of both pressure and RF power applied to the electrodes. Values of Argon pressure used in this work are 0.1, 0.2, 0.3, 0.4 and 0.5 Torr. RF power values applied at each of the pressure values are 25, 50, 75, 100, 125, 150, 175 and 200 W.

As far as the probe data are concerned, and although the automated probe system can give direct results on temperature and density values, some of the results involved many inconsistencies as far as some temperature values and general pressure and RF power dependence. This may be attributed to the fact that the built in software of the system fits the acquired data to the ideal well known, Maxwellian based double probe equation given below to estimate the plasma electron temperature and density [23].

$$I = I_0 \tanh\left(\frac{V}{2T_e}\right) \tag{1}$$

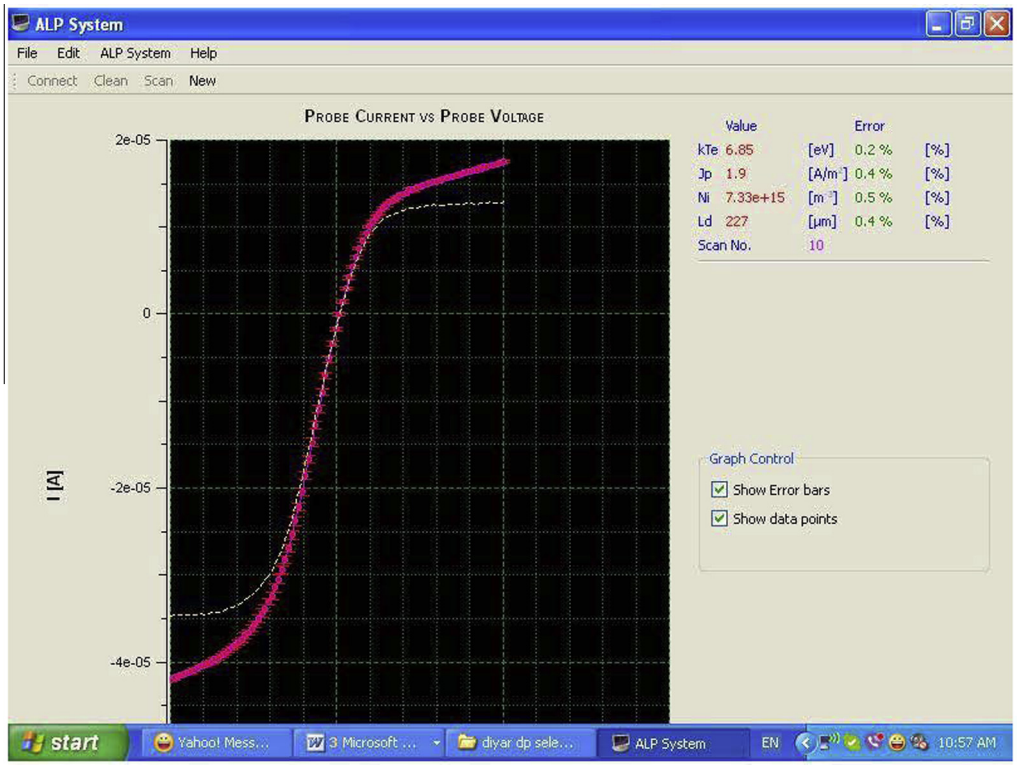

Fig. 2. Typical automated results obtained at pressure of 0.2 Torr and 50 W RF power.

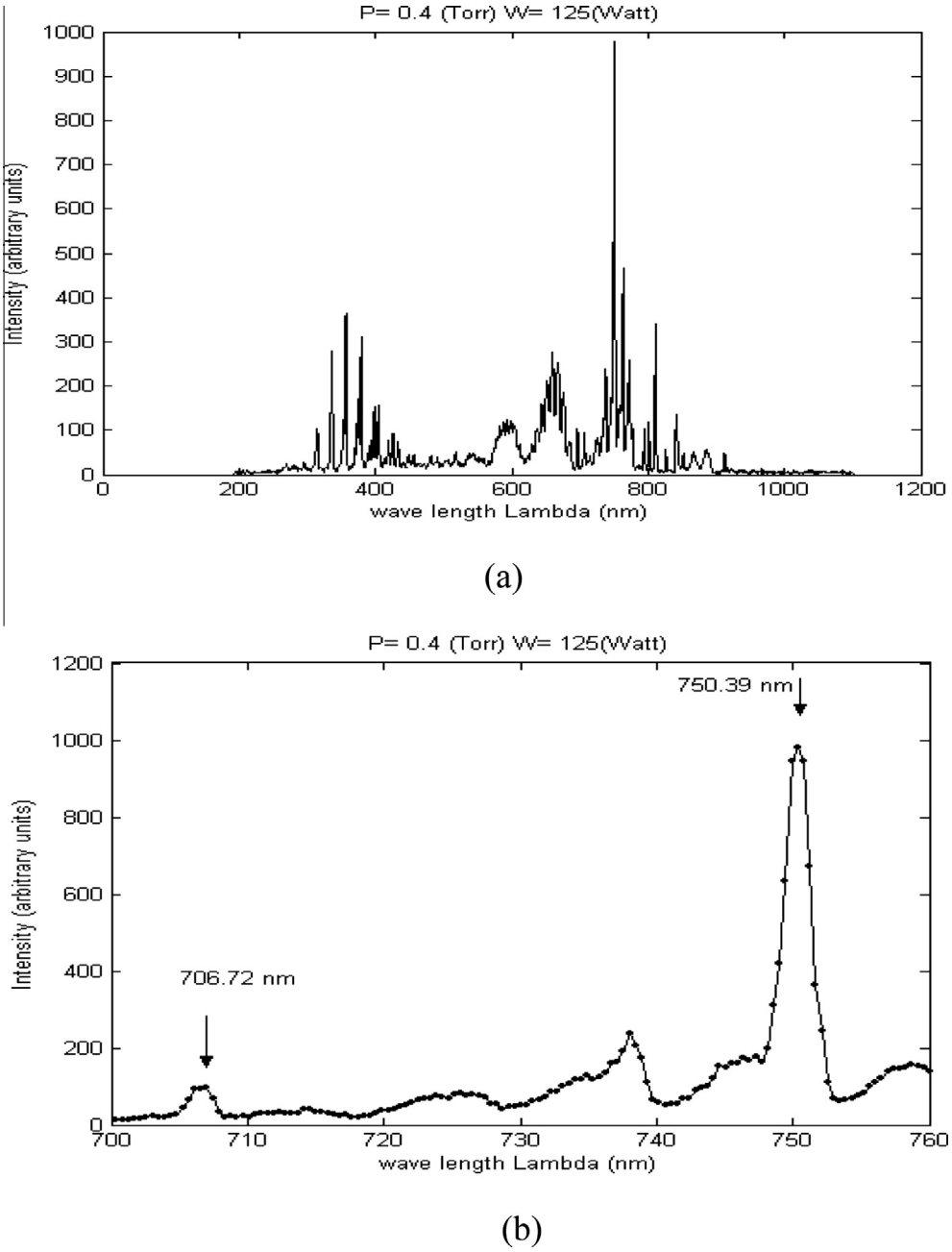

Fig. 3. (a) Typical spectrum obtained at 0.4 Torr, 125 W. (b) Magnified view of the Ar(I) $3p^5(^2P^\circ_{1/2})4p$–$3p^5(^2P^\circ_{3/2})4s$ 706.72 nm and $3p^5(^2P^\circ_{1/2})4p$–$3p^5(^2P^\circ_{1/2})4s$ 750.39 nm lines in the spectrum in (a) used in the calculations.

$$I_0 = 0.61eAN\sqrt{\frac{kT_e}{M_i}} \tag{2}$$

V, I and I_0, are the probe voltage, current, and ion saturation current respectively. N, T_e and M_i, are the plasma electron density, temperature, and the ionic mass respectively.e is the electronic charge, and k is Boltzman's constant.

Eq. (1) gives the highly flat fitted ion saturation current that can be observed as the white line in Fig. 2. Such highly flat ion saturation current behavior is rarely observed experimentally. This is due to two main reasons. The first is related to the fact that Eq. (1) is based on the assumption that the electron distribution function is Maxwellian. This may not be always the case in most plasma. The second is that it does not take into consideration many of the complicated geometrical and plasma sheet effects that take place at the probe tip. In order to overcome such problems, a modified form of Eq. (1) suggested in Ref. [24] is used to fit the data. This equation has the form

$$I = I_0 \tanh\left(\frac{V}{2T_e}\right) + a.V + b \tag{3}$$

a, and b are two additional fitting parameters. The second term on the right of Eq. (3) acts to account for any dynamical effects which cause the ion saturation regions to deviate from the ideal flat voltage dependence. The parameter b accounts for any current offsets within the measuring system. Typical fit of experimental data of Fig. 2 fitted to Eq. (3) is shown in Fig. 4. Similar application of Eq. (3) for all data produced over 95% confidence level fits. The

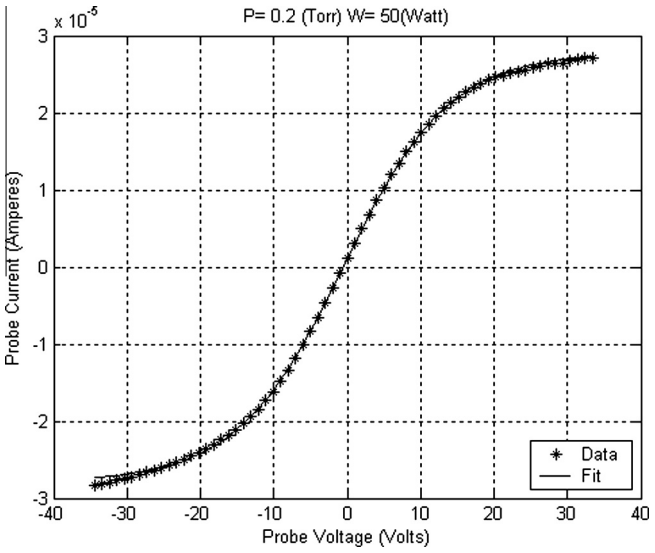

Fig. 4. Experimental double probe data in Fig. 2 fitted to Eq. (3).

plasma electron temperature and density are thus derived from these fits.

Spectral line ratio procedure analysis is applied to the spectroscopic data acquired simultaneously with the probe data. The two lines selected are Ar (I) $3p^5(^2P^\circ_{1/2})4p$–$3p^5(^2P^\circ_{3/2})4s$ 706.72 nm and $3p^5(^2P^\circ_{1/2})4p$–$3p^5(^2P^\circ_{1/2})4s$ 750.39 nm.

Plasma electron density values of the order of $10^{11}/cm^3$ deduced from probe results dictate that the use of the temperature-line ratio equation derived on the bases of the local thermal equilibrium model (LTE) might not prove useful [25]. This equation is

$$kT_e = \frac{E' - E}{\ln(I\lambda^3 g'f'/I'\lambda'^3 gf)} \tag{4}$$

where I, λ, g, f, and E are the total intensity, wavelength, statistical weight, absorption oscillator strength and excitation energy of one of the lines respectively. Primed quantities are those for the second line. These values for the two lines considered are taken from tables of the National Institute of Standards and Technology (NIST) [26].

It may be worth pointing out that the use of Eq. (4) produced considerably low values of the plasma electron temperature in the range of 2–3 eV. This is expected because Eq. (4) which is based on the LTE model is only applicable for plasma electron density value.

$$n_e(\mathrm{cm}^{-3}) \geq 1.6 \times 10^{12}[T_e(eV)]^{1/2} \times [E_{mn}(eV)]^3 \tag{5}$$

E_{mn} is the excitation energy between the two levels.

A more acceptable treatment at the values of plasma electron density considered here may be through the use of equations based on steady state corona model (SSCM) [27]. The plasma electron density constrain on this model is

$$n_e[\mathrm{cm}^{-3}] \leq 5.6 \times 10^8 (z+1)^6 (T_e[eV])^{1/2} \times \exp\left[\frac{1.162 \times 10^3 (z+1)^2}{T_e}\right] \tag{6}$$

Z is the degree of ionization.

Probe temperature and density data suggest that this condition is satisfied for plasma electron temperature values considered here.

The temperature-line ratio equation in this model is given by

$$kT_e = \left[(7.87 \times 10^{-9}) E_\infty^{7/4} \frac{fgI'\lambda'^3}{f'g'I\lambda^3} \exp\left(\frac{E' + E_\infty - E}{kT_e}\right)\right]^{4/3} \tag{7}$$

E_∞ is the ultimate ionization energy.

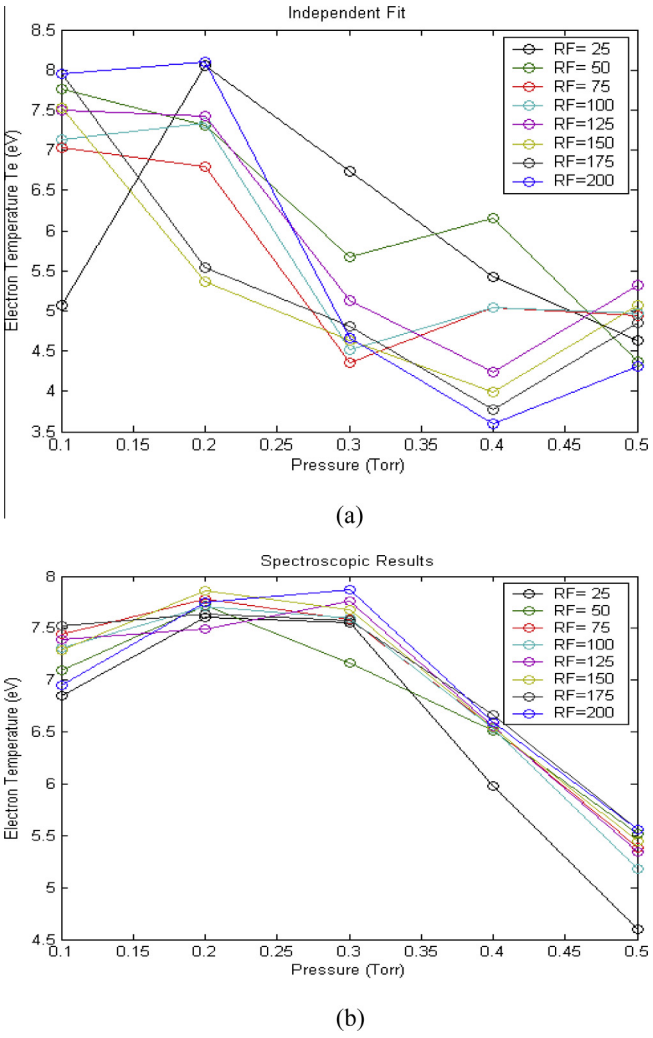

Fig. 5. Pressure dependence at different RF power levels of plasma electron temperatures obtained (a) using double probe. (b) Spectroscopic line ratio.

This equation cannot be solved analytically. However, a solution using Lambert function has been found using MATLAB and a special MATLAB software has been written for the purpose.

Results and discussion

Plasma electron temperature results obtained using both methods described above are presented in Figs. 5 and 6. Data in Fig. 5a and b represent plasma electron temperature versus pressure obtained using probe and spectroscopy methods respectively. Although the spectroscopy results show more monotonic relation to pressure, the probe data tend to show a similar trend but with wider dispersions. The two sets of results show agreeable consistency with absolute mean difference (summed over all measurements) of about 1.2 eV. These differences will be discussed later. However, and as far as the spectroscopy results are concerned, the temperature values at all RF powers tend to show a slight increase up to a pressure value of 0.2–0.3 Torr. This is followed by a significant decrease for pressure values above 0.3 Torr. This effect is also observable in some but not all of the probe data. Considering the more monotonic behavior of the spectroscopy data, it can be speculated that this change in the pressure region of 0.2–0.3 Torr may be interesting. This is because this pressure region is also close to the position of the Paschen minimum for

the electrode setup geometry used. If one accepts such association, this behavior can be explained by the fact that at pressure values above the Paschen minimum, inelastic collisions become more dominant resulting in a decrease of plasma electron temperatures.

Temperature values at all five pressure values obtained by both methods are plotted against RF power in Fig. 6. Comparison between Fig. 6a and b indicates that there is a good consistency between the two sets of results for most pressures and RF power values except those at 0.3 Torr and to a less extent at 0.4 Torr. This may be attributed to the fact that the use of Eq. (7) which is based on the steady state corona model may not have been justified. This will be discussed later in relation to the variation of plasma electron density values.

Fig. 7a and b shows the results of plasma electron density plotted against pressure and RF power respectively. Fig. 7a reflects some interesting Paschen curve related signatures. The first is related to the almost density independence upon pressure for the lowest RF power value of 25 W. This power value is just slightly higher than the minimum power required to produce self-sustained discharge at the Paschen minimum pressure. Change of pressure, which results in a change of collision rate does not result in a change of plasma electron density. This is due to the insufficient pumping of external energy to the discharge. The situation changes as RF power values are increased. For RF powers 50–150 W, the density assumes maximum value near the Paschen minimum of about 0.3 Torr. The excess energy is consumed in the creation of more ion pairs. The situation changes slightly at higher RF powers of 175 and 200 W. The position of maximum density value shifts to about 0.4 Torr. Here one may speculate that these higher power values will enable the discharge to utilize the extra neutral density at a higher power to produce more ion pairs at a higher pressure. This increase is followed by a fall in density values at 0.5 Torr. This is further demonstrated in Fig. 7b where the plasma electron density values show a systematic increase with increasing RF power. The Paschen minimum effect can also be observed in this figure where the density values at 0.3–0.4 Torr are significantly higher than those at other pressures.

Some of the measured plasma density values in Fig. 7 are higher than the constrain value imposed by Eq. (6). This suggests that the use of Eq. (7) in the plasma temperature calculation may not be fully justified. This was checked by recalculating the mean of the absolute differences between temperature values obtained by probe and spectroscopic line ratio methods but without including temperature values associated with density values greater than 8×10^{16} (m^{-1}). This resulted in a drop of value of the absolute mean differences from 1.2 eV mentioned above to about 0.6 eV. This may be considered to form a guideline for the validity range of Eq. (7). It must be pointed out however that the use of the local thermal equilibrium model (Eq. (4)) produced temperature values

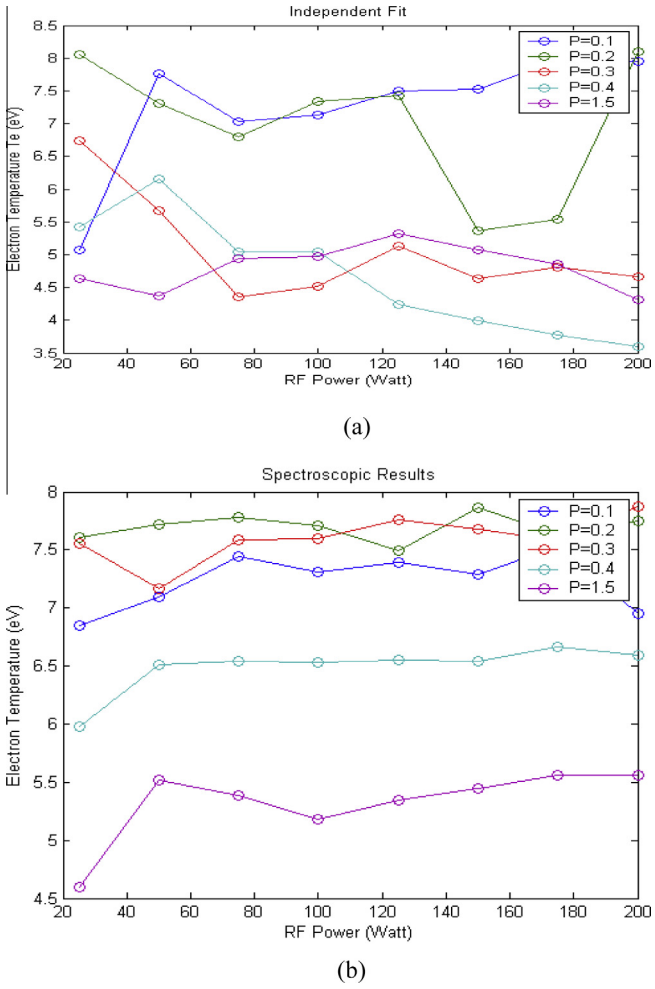

Fig. 6. RF power dependence of plasma electron temperatures at different pressures obtained (a) using double probe. (b) Spectroscopic line ratio.

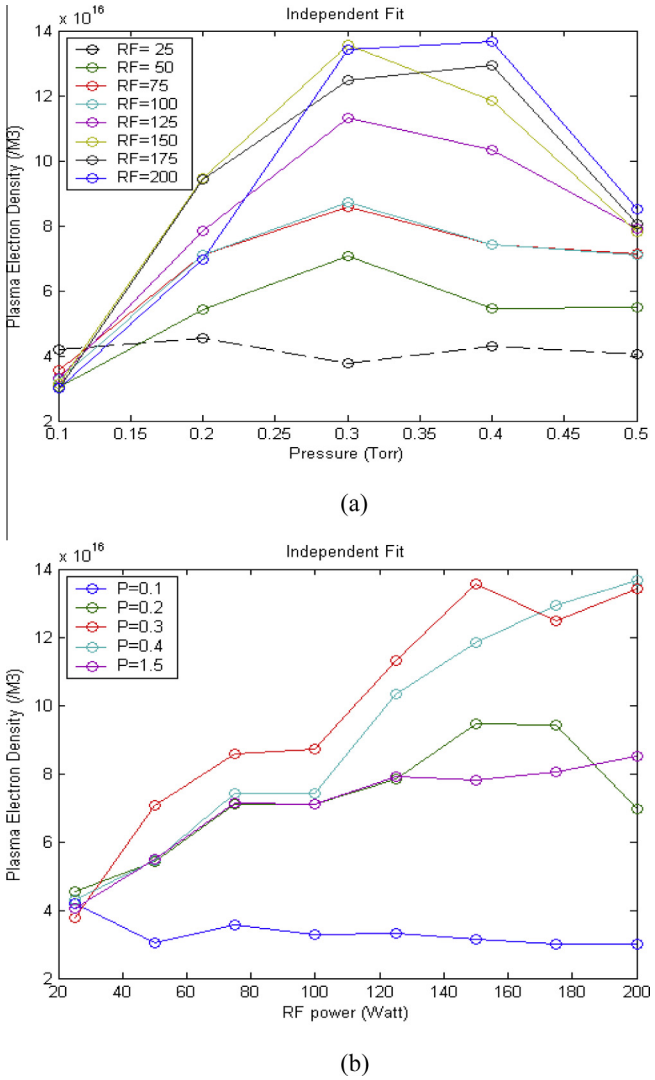

Fig. 7. Plasma electron density plotted against (a) pressure, (b) RF power.

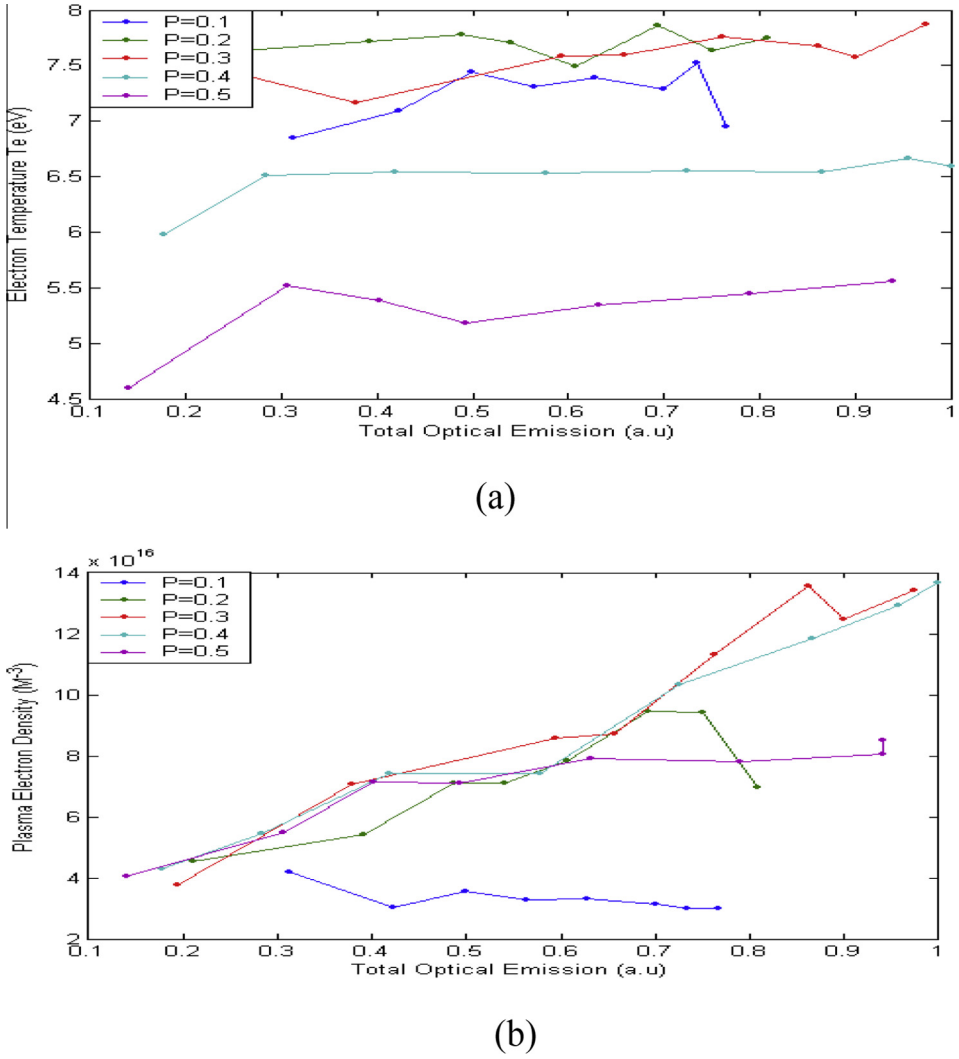

Fig. 8. Dependence of (a) plasma electron temperature, and (b) plasma electron density on total optical emissive of the discharge.

which are too small compared to those obtained by the probe method. This leaves the problem about the using of any of these two extreme models in spectrometric diagnostics at density values suggested by Eqs. (3) and (4) wide open.

One further point worth discussing is the relation between the main two plasma parameters (electron temperature and density) and the total spectral emission (E). The latter is calculated as the total area under the spectrum obtained from the calibrated optical spectrometer. The results are presented in Fig. 8. Fig. 8a demonstrates that T_e does not have any significantly observable dependence on E. This is in contrast to the relation between n_e and E in Fig. 8b where the density shows a systematic increase with the total spectral emission at all pressure values at and to the right of the Paschen minimum. This increase does not seem to be pressure dependent. This may suggest that total spectral emission can be considered as a metric for density measurements but much more theoretical, empirical and experimental considerations are needed in any attempt to build such metric. Even so, the temperature and density data presented here demonstrate two RF discharge properties. The first is plasma electron temperature which is almost independent on both RF power and total spectroscopic emission. The second is that the plasma electron density is strongly correlated to both RF power and total optical emission. This clearly suggests that under the experimental conditions considered here, any additional RF power applied will be mainly consumed in the processes of increasing the plasma electron density rather than increasing electron temperatures.

Conclusion

The main conclusions that can be drawn from this work are:

(1) The plasma electron density constrain on the use of Eq. (7) which is based on the steady state corona model to evaluate plasma temperature using spectral line ration is well described by Eq. (6).
(2) The plasma electron temperature is independent of overall plasma spectral emission.
(3) The plasma electron density pressure variation reflects the Paschen law effect.
(4) The plasma electron density is highly dependent upon the total spectral emission.
(5) RF power applied is mainly consumed to increase the electron density but has little or no effect on electron temperature.

Acknowledgement

We are grateful to the referee for all his dedicated and sincere efforts.

References

[1] Available from: <http://en.wikipedia.org/wiki/ISM_band>.
[2] Beneking C. J Appl Phys 1990;68:4461.
[3] Salabas A, Marques L, Jolly J, Gousset G, Alves LL. J Appl Phys 2004;95:4605.
[4] Radmilović-Radjenović M, Lee JK. Phys Plasmas 2005;12:063501.
[5] Nakano N, Makabe T. J Phys D 1995;28:31–9.
[6] Moon SY, Kim DB, Gweon B, Choea W. Appl Phys Lett 2008;93:221506.
[7] Vahedi V, Birdsall CK, Lieberman MA, DiPeso G, Rognlien TD. Phys Fluids 1993;B(5):2719–29.
[8] Köhler K, Coburn JW, Horne DE, Kay E, Keller JH. J Appl Phys 1985;57:59.
[9] Cox TI, Deshmukh VGI, Hope DAO, Hydes AJ, Braithwaite NSJ, Benjamin NMP. J Phys D: Appl Phys 1987;20:820.
[10] Kohler WE, Seebock RJ, Rebentrost F. J Phys D: Appl Phys 1991;24:252.
[11] Bakker LP, Kroesen GMW, de Hoog FJ. IEEE Trans Plasma Sci 1999;27(3).
[12] Mahoney LJ, Wendt AE, Barrios E, Richards CJ, Shohet JL. J Appl Phys 1994;76(4).
[13] Smith HB, Charles C, Boswell RW. Phys Plasmas 2003;10:3.
[14] Nowling GR, Babayan SE, Jankovic V, Hick RF. Plasma Sources Sci Technol 2002;11:97–103.
[15] Bzenic SA, Radovanov SB, Vrhovac SB, Velikic ZB, Jelenkovic BM. Chem Phys Lett 1991;134.
[16] Jarosz J, Mermet JM, Robin JP. Spectrochim Acta, Part B 1978;33:3–4.
[17] Tyshetskiy YO, Smolyakov AI, Godyak VA. Phys Rev Lett 2003;90:25.
[18] Howling AA, Dorier J-L, Hollenstein C, Kroll U, Finger F. J Vac Sci Technol A 1992;10:1080.
[19] Curtins H, Wyrsch N, Shah A. Electron Lett 1987;23:228.
[20] Heintze M, Zeidlitz R, Bauer GH. J Phys D: Appl Phys 1993;26:1781.
[21] Available from: <http://www.impedans.com/langmuir-probe>.
[22] Available from: <http://www.gmp.ch/hr2000highresolutionminiaturefiberoptic spectrometer-p-932.html>.
[23] Naz MY, Ghaffar A, Rehman NU, Naseer S, Zakaullah M. Prog Electromagnet Res 2011;114:113–28.
[24] Smith BA, Overzet LJ. Rev Sci Instrum 1998;69:1372.
[25] Swift JD, Schwar MJR. Electrical probes for plasma diagnostics. London: Iliffe; 1970.
[26] National Institute of Standards and Technology (NIST). Available from: <http://physics.nist.gov/PhysRefData/Handbook/Tables/argontable3.htm>.
[27] Garamoon AA, Samir A, Elakshar FF, Nosair A, Kotp EF. IEEE Trans Plasma Sci 2007;35(1).